Eur. Phys. J. Plus (2018) **133**: 129
DOI 10.1140/epjp/i2018-11969-0

THE EUROPEAN PHYSICAL JOURNAL PLUS

Regular Article

Bohr Hamiltonian for $\gamma = 30^\circ$ with Davidson potential

Ibrahim Yigitoglu[a] and Melek Gokbulut[b]

Department of Physics, Faculty of Arts and Sciences, Gaziosmanpaşa University, 60250, Tokat, Turkey

Received: 26 January 2018
Published online: 28 March 2018 –

Abstract. A γ-rigid solution of the Bohr Hamiltonian for $\gamma = 30^\circ$ is constructed with the Davidson potential in the β part. This solution is going to be called $Z(4)$-D. The energy eigenvalues and wave functions are obtained by using the analytic method developed by Nikiforov and Uvarov. The calculated intraband and interband $B(E2)$ transitions rates are presented and compared with the $Z(4)$ model predictions. The staggering behavior in γ-bands is considered to search $Z(4)$-D candidate nuclei. A variational procedure is applied to demonstrate that the $Z(4)$ model is a solution of the critical point at the shape phase transition from spherical to rigid triaxial rotor.

1 Introduction

Atomic nuclei exhibit quantum phase transitions between different shapes. The studies investigating the shape phase transitions of atomic nuclei are crucial for providing knowledge of the nuclear structure. The different shapes correspond to dynamical symmetries and they are handled using the interacting boson model (IBM) [1], which is based on the group theoretical framework. The underlying group structure of the model leads to a simple Hamiltonian which is capable of describing collective states in even-even nuclei. There are four dynamical symmetries of the IBM. Out of the four dynamical symmetries, three, called $U(5)$, $SU(3)$ and $SU(3)^*$ limits, correspond to vibrational nuclei with a spherical form, an axially symmetric prolate rotor and an axially symmetric oblate rotor, respectively. The fourth symmetry is located in the middle of $SU(3)$-$SU(3)^*$ and is labelled with $O(6)$, which represents the structure of γ-unstable nuclei [2,3].

The concept of critical point symmetry is introduced to describe nuclei at the phase transitional point. At the critical point of the shape phase transition, where the structure changes most rapidly, the system goes from one symmetry limit to another. All these critical point symmetries are constructed using analytical solutions of the Bohr Hamiltonian [4] that describe the collective motion of nuclei in terms of two-shape variables, the deformation parameter β and a measure of the axial asymmetry γ, and three Euler angles defining the orientation of the deformed nucleus in space.

The $E(5)$ [5] and $X(5)$ [6] critical point symmetries are designed to describe shape phase transitions from spherical ($U(5)$) to γ-unstable ($O(6)$) and from spherical ($U(5)$) to axially symmetric prolate ($SU(3)$) shapes, respectively. The $E(5)$ critical point symmetry is obtained for a γ-independent potential, while the $X(5)$ one is obtained as an approximate solution for $\gamma \approx 0^\circ$. Other critical point symmetries were suggested, called $Y(5)$ [7] and $Z(5)$ [8], to describe the critical points between axial to triaxial deformed shapes and between triaxial vibrator to rigid triaxial rotator, respectively. The $Z(5)$ critical point symmetry, which has no direct solution in the framework of IBM, is obtained as an approximate solution for $\gamma \approx 30^\circ$. Since it is expected that the potential be flat at the point where the shape phase transition occurs [9–11], an infinite square-well potential with respect to the β variable is used in the $E(5)$, $X(5)$ and $Z(5)$ symmetries. Unlike these, the $Y(5)$ critical point symmetry is established considering the harmonic oscillator potential in the β variable and a square well potential in γ variable. In the following years, two γ-rigid solutions are introduced where a harmonic oscillator potential is used for the γ part having a deep minimum at $\gamma = 30^\circ$ and $\gamma = 0^\circ$ by the name of $Z(4)$ [12] and $X(3)$ [13] models, respectively. In these cases, the γ variable is treated as a parameter. Later on, new solutions based on constructing the Bohr Hamiltonian choosing various forms of potentials, such as Morse [14], Kratzer [15–17], Coulomb [15,16], Davidson [16–19], Eckart [20], Manning-Rosen [21], Killingbeck [22] and sextic potentials [23], have been studied to investigate the shape phase transitions between different limiting nuclear structures and to explain the known experimental data in various mass regions.

[a] e-mail: ibrahim.yigitoglu@gop.edu.tr (corresponding author)
[b] e-mail: melek.kgb@gmail.com

In the present work a version of the $Z(4)$ model is introduced by using the Davidson potential [24] in the β-part of the Schrödinger equation. The energy eigenvalues and wave functions are obtained by using the analytical method developed by Nikiforov and Uvarov [25]. $BE(2)$ transitions rates are calculated. This solution is going to be called the $Z(4)$-D model. Davidson-type potentials, having a minimum at $\beta \neq 0$, give rise to exact solutions which cover all the way from $U(5)$ to $O(6)$ and from $U(5)$ to $SU(3)$ [26,27] and allow the use of a variational procedure to find the physical quantities at the critical point. In this article, a variational procedure is applied for recovering the ground state band and γ-band energies of the $Z(4)$ model predictions, in order to determine whether or not the $Z(4)$ model is located at the critical point.

2 The Z(4)-D model

2.1 The energy spectra

According to the Davydov and Chaban approach [28], the nucleus is assumed rigid with respect to γ vibrations. Thus the Hamiltonian depends on four variables (β, θ_i) and is expressed as follows:

$$H = -\frac{\hbar^2}{2B}\left[\frac{1}{\beta^3}\frac{\partial}{\partial\beta}\beta^3\frac{\partial}{\partial\beta} - \frac{1}{4\beta^2}\sum_{\kappa=1}^{3}\frac{Q_\kappa^2}{\sin^2(\gamma - \frac{2\pi}{3}\kappa)}\right] + U(\beta), \tag{1}$$

where β and γ are the usual collective coordinates, while Q_κ $(\kappa = 1, 2, 3)$ are the components of the angular momentum and B is the mass parameter. In the $Z(4)$ model, the potential has a deep minimum at $\gamma = 30^\circ$ and, for this case, one can write the last term in eq. (1) as

$$\sum_{\kappa=1}^{3}\frac{Q_\kappa^2}{\sin^2(\gamma - \frac{2\pi}{3}\kappa)} = 4(Q_1^2 + Q_2^2 + Q_3^2) - 3Q_1^2. \tag{2}$$

Consider the wave function of the form $\Psi(\beta, \theta_i) = \phi(\beta)\psi(\theta_i)$, where θ_i $(i = 1, 2, 3)$ are the Euler angles and with reduced energies $\varepsilon = (2B/\hbar^2)E$ and reduced potentials $u = (2B/\hbar^2)U$. The Schrödinger equation can be separated into two parts

$$\left[\frac{1}{\beta^3}\frac{\partial}{\partial\beta}\beta^3\frac{\partial}{\partial\beta} - \frac{\lambda}{\beta^2} + (\varepsilon - u(\beta))\right]\phi(\beta) = 0, \tag{3}$$

$$\left[\left(Q_1^2 + Q_2^2 + Q_3^2\right) - \frac{3}{4}Q_1^2 - \lambda\right]\psi(\theta_i) = 0. \tag{4}$$

Equation (4) has been solved by Meyer-ter-Vehn [29] and the eigenfunctions and the value of λ have been obtained as follows:

$$\psi\left(\theta_i\right) = \sqrt{\frac{2L+1}{16\pi^2(1+\delta_{\alpha,\mu})}} \times \left[D^L_{\mu,\alpha}(\theta_i) + (-1)^L D^L_{\mu,-\alpha}(\theta_i)\right], \tag{5}$$

$$\lambda = \lambda_{L,\alpha} = L(L+1) - \frac{3}{4}\alpha^2. \tag{6}$$

The eigenvalues of the angular momentum in the intrinsic frame are denoted by L, while the projections of the angular momentum on the body-fixed $\hat{x}'$-axis are denoted by α, which has to be an even integer due to the symmetry [29]. The total wave function is written as

$$\Psi(\beta, \theta_i) = \phi(\beta)\sqrt{\frac{2L+1}{16\pi^2(1+\delta_{\alpha,\mu})}} \times \left[D^L_{\mu,\alpha}(\theta_i) + (-1)^L D^L_{\mu,-\alpha}(\theta_i)\right]. \tag{7}$$

In the present work, the Davidson potential [24] depending on the β variable is considered:

$$u(\beta) = \beta^2 + \frac{\beta_o^4}{\beta^2}. \tag{8}$$

Here β_o indicates the minimum of the potential. By putting eqs. (6) and (8) into eq. (3), this equation can be rewritten as

$$\frac{\mathrm{d}^2\phi(\beta)}{\mathrm{d}\beta^2} + \frac{3}{\beta}\frac{\mathrm{d}\phi(\beta)}{\mathrm{d}\beta} + \left[\varepsilon - \frac{L(L+1)}{\beta^2} + \frac{3}{4\beta^2}\alpha^2 - \beta^2 - \frac{\beta_o^4}{\beta^2}\right]\phi(\beta) = 0. \tag{9}$$

In order to apply the Nikiforov-Uvarov (NU) method, the coordinate transformations, $\beta^2 = z$ and $\phi(\beta) \to \psi(z) = \varphi(z)y_n(z)$, should be done in eq. (9). Then we get

$$\frac{\mathrm{d}^2\psi(z)}{\mathrm{d}z^2} + \frac{4}{2z}\frac{\mathrm{d}\psi(z)}{\mathrm{d}z} + \frac{1}{4z^2}\left[-z^2 + \varepsilon z - \eta\right]\psi(z) = 0, \tag{10}$$

where $\eta = \beta_o^4 + L(L+1) - \frac{3}{4}\alpha^2$.

Equation (10) is in the same form as the following equation:

$$\psi''(z) + \frac{\tilde{\tau}(z)}{\sigma(z)}\psi'(z) + \frac{\tilde{\sigma}(z)}{\sigma^2(z)}\psi(z) = 0, \tag{11}$$

which is a hypergeometic linear diferential equation and closely associated with the NU method. In eq. (11), $\sigma(z)$ and $\tilde{\sigma}(z)$ are polynomials of at most second degree, $\tilde{\tau}(z)$ is a first-degree polynomial and $\psi(z)$ is a function of the hypergeometric type. By comparing eqs. (10) and (11), we determine the parametric polynomials:

$$\tilde{\tau}(z) = 4, \qquad \sigma(z) = 2z, \qquad \tilde{\sigma}(z) = -z^2 + \varepsilon z - \eta. \tag{12}$$

The functions and the parameters required in this method are defined as follows:

$$\begin{aligned}
\pi(z) &= \sigma'(z) - \tilde{\tau}(z)/2 \pm \left[\left(\sigma'(z) - \tilde{\tau}(z)/2\right)^2 - \tilde{\sigma}(z) + k\sigma(z)\right]^{1/2}, \\
\tau(z) &= \tilde{\tau}(z) + 2\pi z, \\
\Omega &= k + \pi'(z), \\
\Omega_n &= -n\tau' - \frac{n(n-1)}{2}\sigma'', \quad n = 0, 1, 2, \ldots.
\end{aligned} \tag{13}$$

Using the parametric polynomials, we found the equalities

$$\begin{aligned}
k_- &= \varepsilon/2 - \sqrt{\eta+1}, \\
\pi(z) &= -1 - \left[z - \sqrt{\eta+1}\right], \\
\tau(z) &= 2 - 2\left[z - \sqrt{\eta+1}\right], \\
\Omega &= \varepsilon/2 - \sqrt{\eta+1} - 1, \\
\Omega_n &= 2n.
\end{aligned} \tag{14}$$

Following the NU method,

$$\begin{aligned}
\frac{\varphi'(z)}{\varphi(z)} &= \frac{\pi(z)}{\sigma(z)}, \\
y_n(z) &= \frac{B_n}{\rho(z)}\frac{\mathrm{d}^n}{\mathrm{d}z^n}\left[\sigma^n(z)\rho(z)\right], \\
\left[\sigma(z)\rho(z)\right]' &= \tau(z)\rho(z),
\end{aligned} \tag{15}$$

we have calculated $\varphi(z)$ and $y_n(z)$ and the eigenfunction is written with respect to the β variable as

$$\phi(\beta) = C_N\beta^a e^{-\beta^2/2}L_n^{a+1}(\beta^2), \tag{16}$$

where C_N is the normalization constant, $a = -1 + \sqrt{\beta_o^4 + \frac{L(L+4)+3n_\omega(2L-n_\omega)+4}{4}}$ and L_n are the Laguerre polynomials. The C_N normalization constant is obtained from the condition $\int_0^\infty \phi^2(\beta)\beta^3\mathrm{d}\beta = 1$. Then, the final expression for the eigenfunction is determined as follows:

$$\phi(\beta) = \left[\frac{2}{\Gamma(a+2)\binom{n+a+1}{n}}\right]^{1/2}\beta^a e^{-\beta^2/2}L_n^{a+1}(\beta^2). \tag{17}$$

Finally, for $\Omega = \Omega_n$ in eq. (14), we obtain the energy eigenvalues as follows:

$$E_{n,L} = 2n + 1 + \sqrt{\beta_o^4 + L(L+1) - \frac{3}{4}\alpha^2 + 1}, \tag{18}$$

where n is the usual oscillator quantum number and β_o specifies to the position of the minimum of the potential. Instead of α, it is convenient to use the wobbling quantum number $n_\omega = L - \alpha$ [29], which labels a series of bands $L = n_\omega, n_\omega + 2, n_\omega + 4, \ldots$ (with $n_\omega > 0$) next to the ground state band (with $n_\omega = 0$). Inserting $\alpha = L - n_\omega$, eq. (18) reads

$$E_{n,L}^{n_\omega} = 2n + 1 + \sqrt{\beta_o^4 + \frac{L(L+4) + 3n_\omega(2L - n_\omega) + 4}{4}}\,. \tag{19}$$

The energy spectra of the $Z(4)$ and of the Davidson cases become directly comparable through the relation $n = s - 1$, where s is labeling the order of zero of the Bessel function and n is labeling the number of zeros of the Laguerre polynomial. Thus, we call it the $Z(4)$-D model. The energy ratios $R_{n,L}^{(n_\omega)}$, which play an important role in investigating the nuclear structure, are defined as

$$R_{n,L}^{(n_\omega)} = \frac{E_{n,L}^{n_\omega} - E_{0,0}^{0}}{E_{0,2}^{0} - E_{0,0}^{0}}\,. \tag{20}$$

The levels of the ground state band are characterized by $s = 1$, $n_\omega = 0$ ($n = 0$), while the quasi-β_1 ones are characterized by $s = 2$, $n_\omega = 0$ ($n = 1$). The quasi-γ_1 band is constituted of even L levels, with $s = 1$, $n_\omega = 2$ and of the odd L levels, with $s = 1$, $n_\omega = 1$.

2.2 B(E2) transition rates

The general form of the quadrupole operator is given by

$$T_\mu^{(E2)} = t\beta \left[D_{\mu,0}^{(2)}(\theta_i) \cos\left(\gamma - \frac{2\pi}{3}\right) + \frac{1}{\sqrt{2}} \left(D_{\mu,2}^{(2)}(\theta_i) + D_{\mu,-2}^{(2)}(\theta_i) \right) \sin\left(\gamma - \frac{2\pi}{3}\right) \right], \tag{21}$$

where t denotes a scalar factor. The number appearing in the Wigner functions next to μ represents the angular momentum quantum number α.

For $\gamma = \pi/6$, eq. (21) has the form

$$T_\mu^{(E2)} = -\frac{t}{\sqrt{2}}\beta \left[D_{\mu,2}^{(2)}(\theta_i) + D_{\mu,-2}^{(2)}(\theta_i) \right]. \tag{22}$$

The electric quadrupole transition rate from an initial to a final state is expressed as

$$B(E2; L_i\alpha_i \to L_f\alpha_f) = \frac{5}{16\pi} \frac{|\langle L_f\alpha_f | T^{(E2)} | L_i\alpha_i \rangle|^2}{2L_i + 1}\,, \tag{23}$$

where, to calculate the reduced matrix elements, the Wigner-Eckart theorem is used:

$$\left\langle L_f\mu_f\alpha_f \left| T_\mu^{(E2)} \right| L_i\mu_i\alpha_i \right\rangle = \frac{\langle L_i 2 L_f | \mu_i \mu \mu_f \rangle}{\sqrt{2L_f + 1}} \left\langle L_f\alpha_f \left| T^{(E2)} \right| L_i\alpha_i \right\rangle. \tag{24}$$

The integral over β has the form

$$I_\beta(nL, n'L') = \int_0^\infty \beta \phi_{nL}(\beta) \phi_{n'L'}(\beta) \beta^3 \mathrm{d}\beta. \tag{25}$$

3 Numerical results and discussion

The $R_{n,L}^{(n_\omega)}$ ratio is one of the important indicators to evaluate the evolution of the nuclear structure. The parameter-dependent models are important to examine how the characteristic structure of the region of interest changes by varying the free parameter. In order to see this, the numerical results for varying β_o parameter of the $Z(4)$-D solution are presented together with the $Z(5)$ model [8], $Z(4)$ model [12] and the rigid triaxial rotor model (RTR) [30,31] predictions in table 1. The notation L_{s,n_ω} is used for the level energies in table 1. The levels of the ground state band are characterized by $s = 1$, $n_\omega = 0$ ($n = 0$) while the quasi-β_1 ones are characterized by $s = 2$, $n_\omega = 0$ ($n = 1$). The quasi-γ_1 band is constituted of the even L levels with $s = 1$, $n_\omega = 2$ and the odd L levels with $s = 1$, $n_\omega = 1$.

Table 1. Comparison of the $R^{(n_\omega)}_{n,L}$ energy ratios of the $Z(4)$-D solution for different β_o values with the $Z(5)$ model, $Z(4)$ model and the rigid triaxial rotor model (RTR) results.

β_o	0	1.5	2	∞	$Z(5)$	$Z(4)$	RTR
L_{s,n_ω}							
$0_{1,0}$	0.000	0.000	0.000	0.000	0.000	0.000	0.000
$2_{1,0}$	1.000	1.000	1.000	1.000	1.000	1.000	1.000
$4_{1,0}$	2.000	2.349	2.512	2.667	2.350	2.226	2.667
$6_{1,0}$	3.000	3.880	4.394	5.000	3.984	3.669	5.000
$8_{1,0}$	4.000	5.510	6.532	8.000	5.877	5.324	8.000
$10_{1,0}$	5.000	7.198	8.847	11.667	8.019	7.188	11.667
$2_{1,2}$	1.646	1.844	1.927	2.000	1.837	1.766	2.000
$3_{1,1}$	2.162	2.588	2.796	3.000	2.597	2.445	3.000
$4_{1,2}$	3.243	4.269	4.893	5.667	4.420	4.051	5.667
$5_{1,1}$	3.359	4.457	5.137	6.000	4.634	4.239	6.000
$6_{1,2}$	4.568	6.463	7.829	10.000	7.063	6.357	10.000
$7_{1,1}$	4.477	6.310	7.619	9.667	6.869	6.188	9.667
$8_{1,2}$	5.782	8.544	10.747	15.000	9.864	8.788	15.000
$9_{1,1}$	5.557	8.155	10.194	14.000	9.318	8.316	14.000
$10_{1,2}$	6.937	10.558	13.652	20.667	12.852	11.378	20.667
$11_{1,1}$	6.616	9.995	12.833	19.000	11.989	10.630	19.000
$0_{2,0}$	2.000	3.648	5.730		3.913	2.954	
$2_{2,0}$	3.000	4.648	6.730		5.697	4.804	
$4_{2,0}$	4.000	5.998	8.243		7.962	6.893	
$6_{2,0}$	5.000	7.529	10.125		10.567	9.215	
$8_{2,0}$	6.000	9.159	12.263		13.469	11.765	
$10_{2,0}$	7.000	10.846	14.578		16.646	14.538	

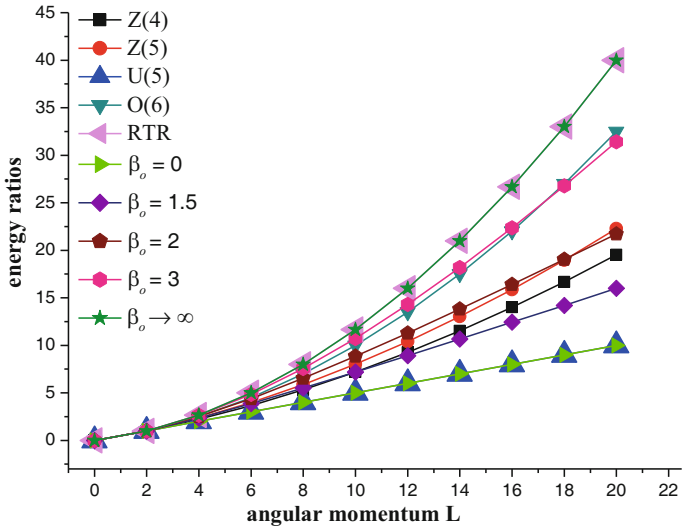

Fig. 1. The energy ratios $R^{(n_\omega)}_{n,L}$ for different β_o values are compared with the $U(5)$, $O(6)$, RTR, $Z(5)$ and $Z(4)$ model predictions. The energy levels of all bands are normalized to the energy of the lowest excited $2_{1,0}$ level.

The comparison of the ground state band energy ratios of the $Z(4)$-D solution for various β_o parameter values are also shown with these model predictions in fig. 1. It is clear that the energy levels for $\beta_o = 0$ correspond to the $U(5)$ vibrational limit, while the rigid triaxial rotor model (RTR) [30,31] predictions, proposed to describe the non-axial nuclei, are obtained for $\beta_o \to \infty$. The energy levels for the $\beta_o = 3$ approach to the $O(6)$ limit structure, while the $Z(5)$ and $Z(4)$ model predictions lie between the spectra obtained for $\beta_o = 1.5$ and $\beta_o = 2$. The spectra obtained with increasing β_o values lie on the way from $U(5)$ to RTR limits.

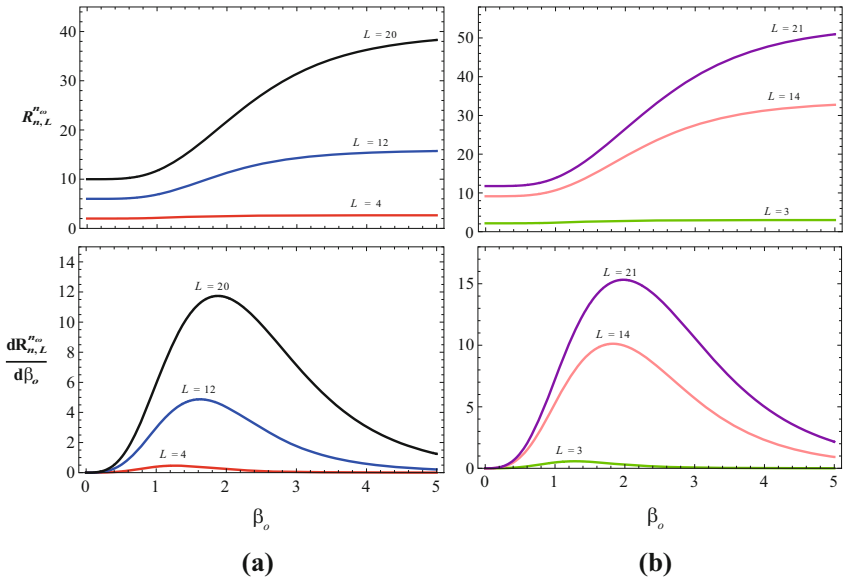

Fig. 2. (a) The $R_{n,L}^{(n_\omega)}$ ratios for ground state bands taking $L = 4, 12, 18$ and their derivatives $\mathrm{d}R_{n,L}^{(n_\omega)}/\mathrm{d}\beta_o$ and (b) the $R_{n,L}^{(n_\omega)}$ ratios for γ_1-bands taking $L = 3, 14, 21$ and their derivatives $\mathrm{d}R_{n,L}^{(n_\omega)}/\mathrm{d}\beta_o$ *versus* the β_o parameter values obtained using the Davidson potential in the $Z(4)$-D model.

Table 2. Values of the $R_{n,L}^{(n_\omega)}$ (var) obtained through the variational procedure for (gsb) and the γ_1-bands are given for comparison reason with the $Z(4)$ model. Here the notation L_{s,n_ω} is used. The angular momentum values corresponding to the gsb band are demonstrated with $s = 1$, $n_\omega = 0$, while the γ_1-bands are demonstrated with $s = 1$, $n_\omega = 2$ for even L and $s = 1$, $n_\omega = 1$ for odd L.

L_{s,n_ω}	$\beta_{o,m}$	$R_{n,L}^{(n_\omega)}$ (var)	$Z(4)$	L_{s,n_ω}	$\beta_{o,m}$	$R_{n,L}^{(n_\omega)}$ (var)	$Z(4)$	L_{s,n_ω}	$\beta_{o,m}$	$R_{n,L}^{(n_\omega)}$ (var)	$Z(4)$
$4_{1,0}$	1.267	2.245	2.226	$2_{1,2}$	1.224	1.776	1.766	$3_{1,1}$	1.286	2.469	2.445
$6_{1,0}$	1.375	3.726	3.669	$4_{1,2}$	1.399	4.120	4.051	$5_{1,1}$	1.410	4.314	4.239
$8_{1,0}$	1.467	5.437	5.324	$6_{1,2}$	1.515	6.508	6.357	$7_{1,1}$	1.508	6.332	6.188
$10_{1,0}$	1.550	7.371	7.188	$8_{1,2}$	1.609	9.038	8.788	$9_{1,1}$	1.592	8.545	8.316
$12_{1,0}$	1.625	9.525	9.256	$10_{1,2}$	1.690	11.743	11.378	$11_{1,1}$	1.668	10.961	10.630
$14_{1,0}$	1.694	11.898	11.526	$12_{1,2}$	1.763	14.637	14.139	$13_{1,1}$	1.738	13.583	13.135
$16_{1,0}$	1.759	14.487	13.996	$14_{1,2}$	1.830	17.730	17.079	$15_{1,1}$	1.803	16.416	15.831
$18_{1,0}$	1.821	17.293	16.665	$16_{1,2}$	1.893	21.026	20.202	$17_{1,1}$	1.864	19.460	18.719
$20_{1,0}$	1.880	20.316	19.530	$18_{1,2}$	1.952	24.532	23.509	$19_{1,1}$	1.922	22.718	21.799
				$20_{1,2}$	2.009	28.248	27.003	$21_{1,1}$	1.979	26.191	25.071

In the present work, we applied a variational procedure [26,27] to the energy ratios $R_{n,L}^{(n_\omega)}$ of the ground state (gsb) and γ_1-bands. The variational procedure was proposed to determine the physical quantities at the point of shape phase transitions in nuclei. The variational procedure applied here resembles that of the Ritz method in quantum mechanics [32]. In the present case, it is achieved by maximizing the rate of change of the physical quantity while, in the Ritz method, the energy is minimized. For this purpose, a potential with one free parameter which covers the whole range of interest between two limiting structures is selected.

As can be seen in figs. 2(a) and (b), the $R_{n,L}^{(n_\omega)}$ ratios increase with β_o. The increase in the curve corresponding to the $\beta_{o,m}$ value is very steep, where the first derivative $\mathrm{d}R_{n,L}^{(n_\omega)}/\mathrm{d}\beta_o$ has a sharp maximum and the second derivative $\mathrm{d}^2R_{n,L}^{(n_\omega)}/\mathrm{d}\beta_o^2$ vanishes.

Considering that the physical quantities change very rapidly at the point of the shape phase transition, the parameter, $\beta_{o,m}$, corresponding to the maximum value of the rate of change of the physical quantity for each value of angular momentum is determined separately.

The $R_{n,L}^{(n_\omega)}$ (labeled as var) values occurring at $\beta_{o,m}$ points for the ground state and the γ_1-bands are given with the $Z(4)$ model [12] predictions in table 2. The variational procedure results in table 2 show good agreement in ground state and γ_1-bands with the $Z(4)$ model [12] predictions. This agreement could be an evidence of that the $Z(4)$ model is a critical point symmetry between spherical and rigid triaxial rotor model (RTR) [30,31] shapes.

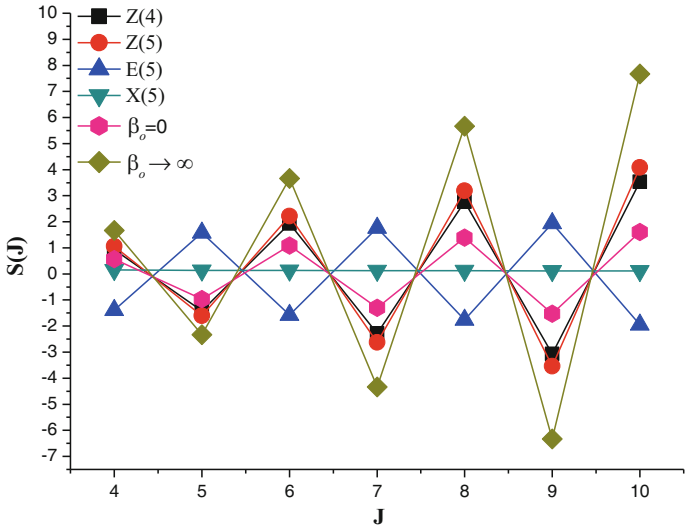

Fig. 3. The $S(J)$ staggering values in the γ_1-band of the $Z(4)$-D solution obtained for $\beta_o = 0$ and $\beta_o \to \infty$ is compared with the $X(5)$, $E(5)$, $Z(5)$ and $Z(4)$ models.

The degree of deviation from asymmetry is usually specified by the γ parameter. The $\gamma = 0°$ limit represents axially symmetric prolate shapes, whereas the $\gamma = 60°$ limit corresponds to axially symmetric oblate shapes. Intermediate values $0° < \gamma < 60°$ are related triaxial shapes and the nucleus possess large asymmetry for $\gamma \approx 30°$. Triaxial deformation has been investigated using two models within the framework of the Bohr Hamiltonian; the rigid-triaxial rotor model of Davydov and Filippov (DF) [30] and the γ-unstable (or γ-soft) rotor model of Wilets and Jean (WJ) [33]. In the former case, the nucleus has a large nonzero fixed γ value where the potential has a deep minimum. In the latter case, the nucleus oscillates in a nearly γ-independent potential between $\gamma = 0°$ and $60°$, the potential is flat in the γ degree of freedom.

The predictions of both models are similar, therefore, these two asymmetric cases can be distinguished by considering the staggering behavior in the quasi-γ bands. In the triaxial $\gamma \approx 30°$ rotor, the γ-band levels cluster according to spins $(2^+_\gamma, 3^+_\gamma)$, $(4^+_\gamma, 5^+_\gamma)$, $(6^+_\gamma, 7^+_\gamma)$, ..., while, in the γ-soft limit, the γ-band levels cluster as 2^+_γ, $(3^+_\gamma, 4^+_\gamma)$, $(5^+_\gamma, 6^+_\gamma)$, ... The staggering behavior can be expressed in terms of the following differential quantity [34,35]:

$$S(J) = \frac{\{E(J^+_\gamma) - E[(J-1)^+_\gamma]\} - \{E[(J-1)^+_\gamma] - E[(J-2)^+_\gamma]\}}{E(2^+_1)}. \tag{26}$$

Both models exhibit exactly opposite staggering behavior in the quasi-γ bands. For the triaxial case, the values of $S(J)$ are positive at even L and negative at odd L while, for the γ-soft shapes, the values of $S(J)$ are positive at odd L and negative at even L. Also, in the limit of an axially symmetric deformed rotor, the $S(J)$ values are positive, small and constant as a function of L [35]. Therefore, the staggering of the odd and even spin levels of a γ-band can be considered as an important structural indicator. This situation can be clearly seen in fig. 3. The $S(J)$ predictions of the $Z(4)$ and $Z(5)$ models are positive at even L and negative at odd L, as can be observed in the triaxial case, while the $S(J)$ values of the $E(5)$ model are negative at even L and positive at odd L as in the γ-soft case. In the $X(5)$ model the $S(J)$ values are positive and nearly constant.

We firstly investigated the staggering behavior in $S(J)$ in the experimental data of the $^{74-76}$Ge, $^{130-132}$Xe, $^{110-114}$Ru, $^{192-198}$Pt, ^{192}Os, ^{166}Er, ^{170}Er and ^{232}Th isotopes. The staggering in γ_1-bands for the $^{74-76}$Ge, $^{110-114}$Ru, ^{192}Pt, ^{192}Os, ^{166}Er, ^{170}Er and ^{232}Th isotopes is compatible with triaxial shapes. This situation is clearly seen in fig. 4. There is not enough experimental data to analyze the behavior of $S(J)$ for the $^{130-132}$Xe and $^{194-198}$Pt isotopes γ_1-bands.

The ^{166}Er, ^{170}Er and ^{232}Th isotopes with the ratios $R^{(0)}_{0,4}$ ($R_{4/2}$) 3.289, 3.310 and 3.284, respectively, also show staggering behavior. However, these $R^{(0)}_{0,4}$ ratios are much higher than in the $Z(4)$-D model predictions and these nuclei can be considered as candidates for $Y(5)$ critical point symmetry at shape phase transition from an axial to triaxial deformed shapes.

The gsb energies obtained for different β_o values are compared with existing experimental data for the $^{74-76}$Ge, $^{192-198}$Pt isotopes, in fig. 5, and for the $^{110-114}$Ru, $^{130-132}$Xe and ^{192}Os isotopes in fig. 6. The $Z(5)$ and $Z(4)$ model predictions are also placed in the figures for comparison.

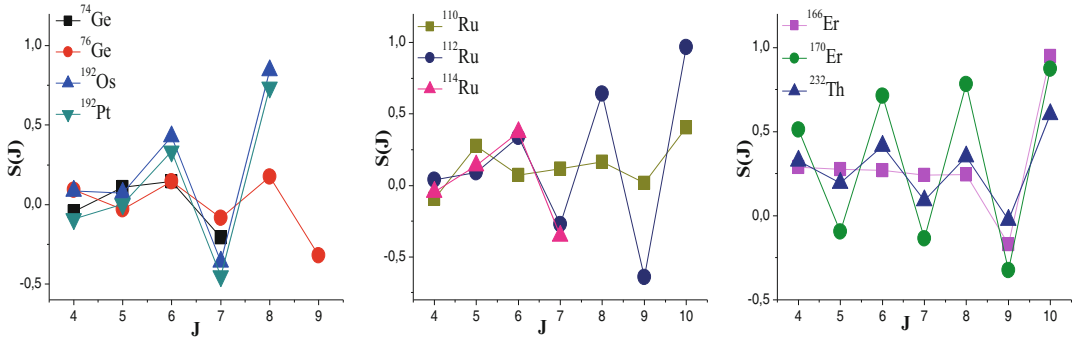

Fig. 4. Experimental $S(J)$ data for ^{74}Ge, ^{76}Ge, ^{192}Os, ^{192}Pt, $^{110-114}$Ru, ^{166}Er, ^{170}Er, ^{232}Th are positive at even L and negative at odd L.

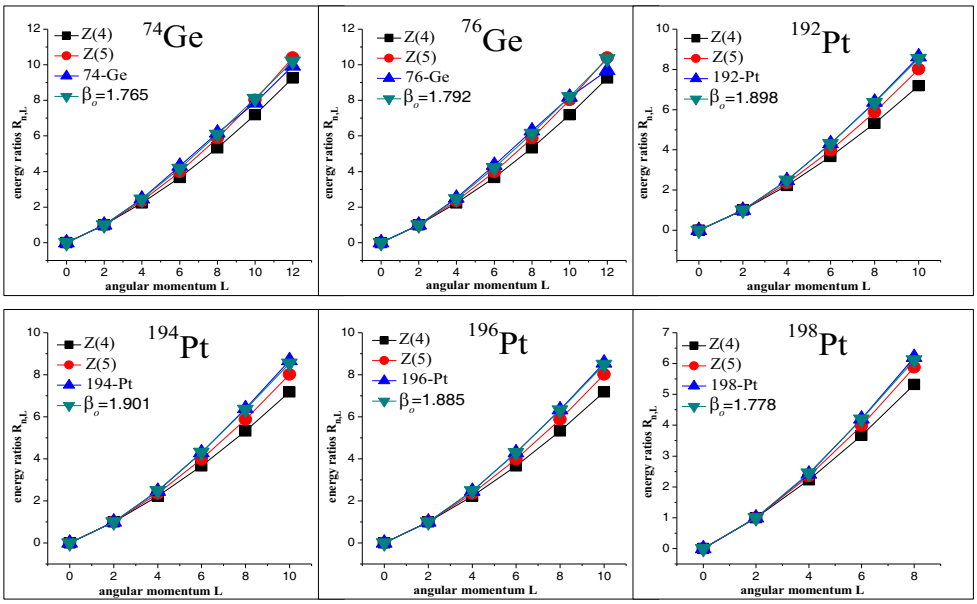

Fig. 5. Comparison of the $Z(4)$-D model gsb energy predictions calculated for different β_o values with $^{74-76}$Ge and $^{192-198}$Pt. The $Z(5)$ and $Z(4)$ model predictions are also placed for comparison.

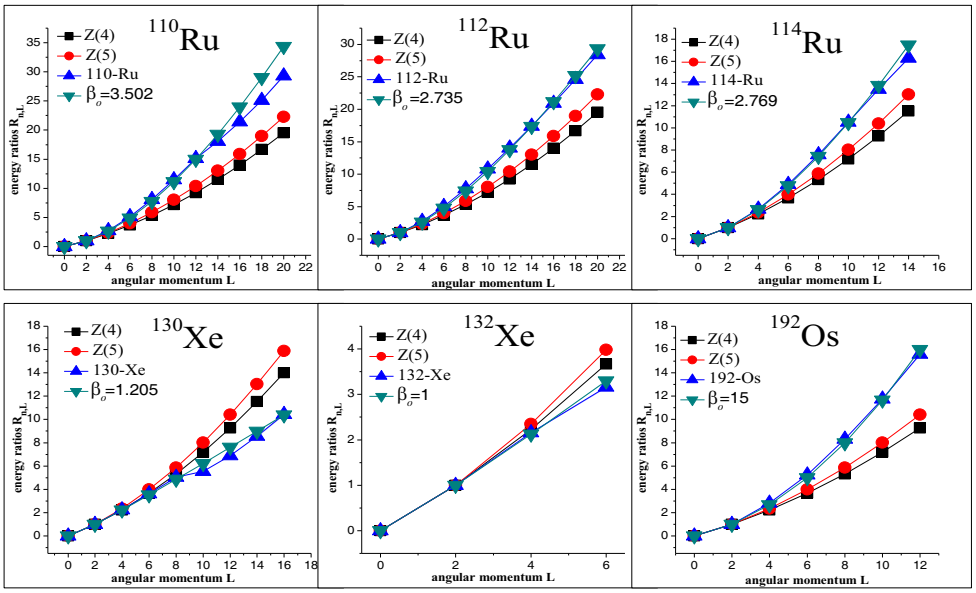

Fig. 6. The $Z(4)$-D model ground state band energy predictions obtained for different β_o values are compared with the data for $^{110-114}$Ru, $^{130-132}$Xe and ^{192}Os. The $Z(5)$ and $Z(4)$ model predictions are also shown for comparison.

Table 3. The theoretical predictions of the $Z(4)$-D model, labeled by the relevant β_o values, with the experimental γ_1-band energies of ^{74}Ge, ^{76}Ge, ^{192}Pt, ^{194}Pt and ^{196}Pt and $Z(4)$ model results.

L_{s,n_ω}	^{74}Ge	^{74}Ge	^{76}Ge	^{76}Ge	^{192}Pt	^{192}Pt	^{194}Pt	^{194}Pt	^{196}Pt	^{196}Pt	
β_o	Exp.	1.765	Exp.	1.792	Exp.	1.898	Exp.	1.901	Exp.	1.885	$Z(4)$
$2_{1,2}$	2.021	1.895	1.969	1.900	1.935	1.915	1.894	1.915	1.936	1.913	1.766
$3_{1,1}$	2.849	2.713	2.735	2.724	2.910	2.763	2.809	2.764	2.854	2.759	2.445
$4_{1,2}$	3.633	4.630	3.592	4.663	3.795	4.786	3.743	4.790	3.636	4.772	4.051
$5_{1,1}$	4.526	4.849	4.418	4.885	4.682	5.020	4.563	5.023	4.526	5.004	4.239
$6_{1,2}$	5.564	7.225	5.390	7.299	5.905	7.578			5.644	7.545	6.357
$7_{1,1}$	6.395	7.042	6.276	7.113	6.677	7.380					6.188
$8_{1,2}$			7.337	9.864	8.186	10.324			7.730	10.269	8.788
$9_{1,1}$			8.077	9.381							8.316

The ^{74}Ge and ^{76}Ge ground state band energies are in better agreement with the $Z(4)$-D solution for $\beta_o = 1.765$ and $\beta_o = 1.792$, respectively, than with the $Z(5)$ and $Z(4)$ model predictions. The $^{192-198}$Pt isotopes gsb data are well produced with $Z(4)$-D (with $\beta_o = 1.898$, $\beta_o = 1.901$, $\beta_o = 1.885$ and 1.778, respectively).

The gsb energies obtained for different β_o values are compared with the existing experimental data for the $^{110-114}$Ru, $^{130-132}$Xe and ^{192}Os isotopes in fig. 6. The gsb energies corresponding to the $Z(4)$-D model show the best agreement with the experimental data of the ^{112}Ru isotope among the nuclei in fig. 6. The ^{110}Ru and ^{114}Ru gsb energies are consistent with the $Z(4)$-D solution up to the $L = 12$ spin for $\beta_o = 3.502$ and $\beta_o = 2.769$, respectively. The ^{130}Xe and ^{132}Xe gsb energies are consistent with both the $Z(4)$ model and the $Z(4)$-D solution obtained for $\beta_o = 1.205$ and $\beta_o = 1$, respectively. The $Z(4)$-D solution is becoming compatible at high β_o values with ^{192}Os.

The β_o values that are used to obtain gsb band energies are also taken into account to calculate γ_1-band energies. The γ_1-band energies obtained for the $Z(4)$-D model with the $^{74-76}$Ge, $^{192-196}$Pt isotopes existing experimental data are listed in table 3 with the $Z(4)$ model predictions.

The γ_1-band energies corresponding to angular momentum values of $2_{1,2}$, $3_{1,1}$, and $5_{1,1}$ for ^{74}Ge and ^{76}Ge isotopes are compatible with the $Z(4)$-D model predictions, while the other γ_1-band energies are compatible with the $Z(4)$ model predictions. The γ_1-band energies, with the spin levels $2_{1,2}$, $3_{1,1}$ and $5_{1,1}$, belonging to ^{192}Pt are consistent with the $Z(4)$-D model, while the energies for the $4_{1,2}$, $6_{1,2}$ and $8_{1,2}$ spin levels are consistent with the $Z(4)$ model predictions. The γ_1-bands energies of $^{194-196}$Pt isotopes for $2_{1,2}$ and $3_{1,1}$ are compatible with $Z(4)$-D, while the $4_{1,2}$ and $5_{1,1}$ level energies are in agreement with the $Z(4)$ model results.

The theoretical predictions of the $Z(4)$-D model, labeled by the relevant β_o values, compared to the experimental γ_1-band energies of $^{110-114}$Ru, ^{192}Os and $^{130-132}$Xe are presented in table 4. The γ_1-band energies concerning the band head and the odd angular momentum values for $^{110-114}$Ru isotopes exhibit similar behavior with the numerical results of the $Z(4)$-D model, while the γ_1-band energies with even spins are consistent with the $Z(4)$ model results. In the case of ^{192}Os, the γ_1-band energies for $2_{1,2}$, $3_{1,1}$ and $5_{1,1}$ are compatible with $Z(4)$-D while the energy for the angular momentum value of $4_{1,2}$ shows good agreement with the $Z(4)$ model. As can be concluded from the values given in table 3 and table 4, the $Z(4)$-D solution predicts γ_1-band heads for these nuclei better than the $Z(4)$ model, except for the $^{130-132}$Xe isotopes.

The gsb and γ_1-band energy values for the $Z(4)$-D solution are given, with the $Z(4)$-sextic predictions and the available experimental data for $^{130-132}$Xe and $^{192-196}$Pt, in table 5. The gsb and γ_1-band energy ratios of the $^{192-196}$Pt isotopes have similar predictions in the $Z(4)$ and $Z(4)$-S models, while the gsb band energy values are well reproduced by the $Z(4)$-D solution. The three models have similar predictions for the ^{130}Xe isotope for gsb band energy values up to spin $L = 8$, however, the γ_1-band energy values are inconsistent with these three model predictions, except for the energy of the angular momentum value $5_{1,1}$, which is compatible with the $Z(4)$-D and $Z(4)$-S results. Although both the $Z(4)$-D and $Z(4)$-S models gsb energy predictions are similar, the $Z(4)$-S model shows relatively good agreement with the Xe isotope. The γ_1-band predictions of all three models are incompatible with ^{132}Xe.

Intraband and interband $B(E2)$ transition rates are also an important indicator for the nuclear structure, since they are sensitive to shape phase transitions. The $B(E2)$ rates of the $Z(4)$-D model for different β_o values are reported in table 6, together with the $Z(4)$ model predictions. The $B(E2)$ rates are normalized to the $B(E2; 2_{1,0} \rightarrow 0_{1,0})$ transition rate value from the lowest excited state to the ground state.

The intraband $B(E2)$ predictions of the $Z(4)$ model for gsb lie between $\beta_o = 1$ and $\beta_o = 1.5$ for low spin values while, with increasing spins, they approach to the predictions of the $Z(4)$-D solution obtained with $\beta_o = 2$. The γ_1-band $B(E2)$ values are compatible with the $Z(4)$-D predictions between $\beta_o = 1$ and $\beta_o = 2$. The interband $B(E2)$ rates from γ_1-band to gsb lie between $\beta_o = 1$ and $\beta_o = 1.5$ and with increasing the spin they approach to $\beta_o = 2$ predictions.

Table 4. The theoretical predictions of the $Z(4)$-D model, labeled by the relevant β_o values, with the experimental γ_1-band energies of $^{110-114}$Ru, ^{192}Os and $^{130-132}$Xe.

L_{s,n_ω}	^{110}Ru	^{110}Ru	^{112}Ru	^{112}Ru	^{114}Ru	^{114}Ru	^{192}Os	^{192}Os	
β_o	Exp.	3.502	Exp.	2.735	Exp.	2.769	Exp.	15.000	$Z(4)$
$2_{1,2}$	2.546	1.990	2.212	1.975	2.124	1.976	2.376	2.000	1.766
$3_{1,1}$	3.572	2.971	3.158	2.928	3.124	2.931	3.355	3.000	2.445
$4_{1,2}$	4.505	5.543	4.143	5.366	4.080	5.378	4.420	5.666	4.051
$5_{1,1}$	5.713	5.860	5.219	5.661	5.176	5.675	5.557	6.000	4.239
$6_{1,2}$	6.997	9.595	6.634	9.062	6.642	9.098	7.120	9.999	6.357
$7_{1,1}$	8.395	9.289	7.779	8.788	7.757	8.822	8.323	9.665	6.188
$8_{1,2}$	9.957	14.095	9.563	12.999			10.369	14.997	8.788
$9_{1,1}$	11.535	13.209	10.707	12.236					8.316
$10_{1,2}$	13.518	18.991	12.817	17.124					11.378
$11_{1,1}$	15.067	17.572	13.902	15.943					10.630
$12_{1,2}$	17.255	24.237	16.354	21.399					14.139
$13_{1,1}$	18.926	22.330	17.303	19.860					13.135
$14_{1,2}$	21.289	29.792	20.128	25.793					17.079
$15_{1,1}$	23.030	27.441	20.916	23.948					15.831
$16_{1,2}$			24.086	30.285					20.202
$17_{1,1}$			24.747	28.175					18.719
L_{s,n_ω}	^{130}Xe	^{130}Xe	^{132}Xe	^{132}Xe					
β_o	Exp.	1.205	Exp.	1.000					$Z(4)$
$2_{1,2}$	2.093	1.771	1.944	1.721					1.766
$3_{1,1}$	3.046	2.423	2.701	2.315					2.445
$4_{1,2}$	3.374	3.841	2.940	3.583					4.051
$5_{1,1}$	4.051	3.996	3.246	3.721					4.239

Table 5. The ground state and γ_1-bands energy ratios ($R^{(n_\omega)}_{n,L}$) obtained by the $Z(4)$-D solution with the $Z(4)$-S (S: sextic potential) model predictions and the available experimental data for $^{130-132}$Xe, $^{192-196}$Pt.

Nucl.	$R^{(0)}_{0,4}$	$R^{(0)}_{0,6}$	$R^{(0)}_{0,8}$	$R^{(0)}_{0,10}$	$R^{(0)}_{0,12}$	$R^{(2)}_{0,2}$	$R^{(1)}_{0,3}$	$R^{(2)}_{0,4}$	$R^{(1)}_{0,5}$	$R^{(2)}_{0,6}$	$R^{(1)}_{0,7}$	$R^{(2)}_{0,8}$
^{130}Xe	2.247	3.627	5.031	5.545	6.890	2.093	3.046	3.373	4.051			
$Z(4)$-D	2.216	3.518	4.861	6.225	7.602	1.771	2.423	3.841	3.996			
$Z(4)$-S	2.415	3.534	5.192	6.402	8.262	1.612	2.180	3.936	4.005			
^{132}Xe	2.157	3.163				1.944	2.701	2.940	3.246			
$Z(4)$-D	2.127	3.296				1.721	2.315	3.583	3.721			
$Z(4)$-S	2.123	3.156				1.532	2.075	3.368	3.475			
^{192}Pt	2.479	4.314	6.377	8.624		1.935	2.910	3.795	4.682	5.905	6.677	8.186
$Z(4)$-D	2.487	4.308	6.350	8.539		1.915	2.763	4.786	5.020	7.578	7.380	10.324
$Z(4)$-S	2.439	3.787	5.773	7.350		1.653	2.302	4.229	4.342	6.358	6.065	9.163
^{194}Pt	2.470	4.298	6.392	8.672		1.894	2.809	3.743	4.563			
$Z(4)$-D	2.488	4.311	6.357	8.552		1.915	2.764	4.790	5.023			
$Z(4)$-S	2.415	3.835	5.880	7.573		1.661	2.332	4.268	4.402			
^{196}Pt	2.465	4.290	6.333	8.558		1.936	2.854	3.636	4.526	5.644		7.730
$Z(4)$-D	2.484	4.296	6.326	8.499		1.913	2.759	4.772	5.004	7.545		10.269
$Z(4)$-S	2.513	3.709	5.579	6.914		1.646	2.249	4.179	4.243	6.041		8.564

Table 6. Intraband and interband $B(E2)$ transition rates for the $Z(4)$-D model corresponding to different β_o values. The gsb is characterized by $s = 1$, $n_\omega = 0$ ($n = 0$), the quasi-β_1 is characterized by $s = 2$, $n_\omega = 0$ ($n = 1$), while the quasi-γ_1 band with even L levels by $s = 1$, $n_\omega = 2$ and the odd L levels by $s = 1$, $n_\omega = 1$. The notation L_{s,n_ω} is used.

β_o	0	1	1.5	2		β_o	0	1	1.5	2	
$L^{(i)}_{s,n_\omega} \to L^{(f)}_{s,n_\omega}$					$Z(4)$	$L^{(i)}_{s,n_\omega} \to L^{(f)}_{s,n_\omega}$					$Z(4)$
$2_{1,0} \to 0_{1,0}$	1.000	1.000	1.000	1.000	1.000	$2_{2,0} \to 0_{2,0}$	1.500	1.485	1.401	1.292	0.769
$4_{1,0} \to 2_{1,0}$	2.083	1.866	1.625	1.499	1.706	$4_{2,0} \to 2_{2,0}$	2.778	2.485	2.126	1.879	1.271
$6_{1,0} \to 4_{1,0}$	3.462	2.992	2.404	2.058	2.414	$6_{2,0} \to 4_{2,0}$	4.327	3.739	2.987	2.504	1.793
$8_{1,0} \to 6_{1,0}$	4.779	4.068	3.127	2.528	2.913	$8_{2,0} \to 6_{2,0}$	5.735	4.881	3.744	2.995	2.177
$10_{1,0} \to 8_{1,0}$	6.071	5.127	3.841	2.980	3.293	$10_{2,0} \to 8_{2,0}$	7.083	5.981	4.476	3.454	2.484
$12_{1,0} \to 10_{1,0}$	7.350	6.178	4.554	3.431	3.597						
$14_{1,0} \to 12_{1,0}$	8.621	7.225	5.270	3.888	3.849						
$16_{1,0} \to 14_{1,0}$	9.886	8.270	5.989	4.349	4.061						
$4_{1,2} \to 2_{1,2}$	1.064	0.932	0.775	0.687	0.801	$5_{1,1} \to 3_{1,1}$	1.983	1.709	1.364	1.158	1.356
$6_{1,2} \to 4_{1,2}$	1.916	1.628	1.245	0.999	1.142	$7_{1,1} \to 5_{1,1}$	3.507	2.975	2.264	1.802	2.049
$8_{1,2} \to 6_{1,2}$	3.447	2.903	2.155	1.645	1.767	$9_{1,1} \to 7_{1,1}$	4.970	4.187	3.111	2.378	2.565
$10_{1,2} \to 8_{1,2}$	4.970	4.168	3.047	2.259	2.266	$11_{1,1} \to 9_{1,1}$	6.384	5.357	3.924	2.920	2.967
$12_{1,2} \to 10_{1,2}$	6.458	5.403	3.915	2.847	2.669	$13_{1,1} \to 11_{1,1}$	7.762	6.498	4.717	3.445	3.290
$3_{1,1} \to 2_{1,2}$	3.207	2.795	2.295	2.019	2.365	$2_{1,2} \to 2_{1,0}$	2.123	1.898	1.649	1.525	1.737
$5_{1,1} \to 4_{1,2}$	2.412	2.049	1.567	1.260	1.452	$4_{1,2} \to 4_{1,0}$	0.544	0.471	0.379	0.325	0.381
$7_{1,1} \to 6_{1,2}$	2.671	2.250	1.674	1.283	1.615	$6_{1,2} \to 6_{1,0}$	0.352	0.300	0.232	0.189	0.218
$9_{1,1} \to 8_{1,2}$	2.763	2.318	1.699	1.265	1.448	$8_{1,2} \to 8_{1,0}$	0.257	0.218	0.164	0.128	0.143
$11_{1,1} \to 10_{1,2}$	2.794	2.339	1.698	1.240	1.305	$10_{1,2} \to 10_{1,0}$	0.202	0.170	0.126	0.096	0.102
$13_{1,1} \to 12_{1,2}$	2.800	2.340	1.688	1.216	1.185	$12_{1,2} \to 12_{1,0}$	0.166	0.139	0.102	0.076	0.076
$3_{1,1} \to 4_{1,0}$	1.916	1.658	1.337	1.155	1.360						
$5_{1,1} \to 6_{1,0}$	1.751	1.490	1.145	0.928	1.074						
$7_{1,1} \to 8_{1,0}$	1.649	1.392	1.042	0.809	0.897						
$9_{1,1} \to 10_{1,0}$	1.580	1.328	0.979	0.737	0.775						
$11_{1,1} \to 12_{1,0}$	1.532	1.284	0.936	0.690	0.684						
$13_{1,1} \to 14_{1,0}$	1.495	1.251	0.906	0.657	0.614						

The $E2$ strength of the $4_{1,0} \to 2_{1,0}$ transition increases in the spherical-to-deformed transition, but the ratio $B_{4/2}(B(E2; 4_{1,0} \to 2_{1,0})/B(E2; 2_{1,0} \to 0_{1,0}))$ decreases [36]. The decreasing $B(E2)$ ratios with increasing β_o obtained in the $Z(4)$-D solution supports this behavior as can be seen in table 6.

4 Conclusion

A γ-rigid solution of the Bohr Hamiltonian is obtained for $\gamma = 30^\circ$ by choosing the Davidson potential in the β part. This solution is called $Z(4)$-D. The separation of variables is exactly achieved. The energy eigenvalues and wave functions are obtained by using the analytic method developed by Nikiforov and Uvarov. $B(E2)$ transition rates are determined. The energy staggering in gamma bands, which is considered as a key signature to distinguish the rigid triaxial and gamma soft structures, has been calculated to search the $Z(4)$-D candidate nuclei. A variational procedure was applied to determine whether or not $Z(4)$ is a solution for the critical point. The variational procedure results show good agreement in ground state and γ_1-bands with the $Z(4)$ model predictions. This agreement indicates that the $Z(4)$ model is a solution for critical point symmetry. The $Z(4)$-D model can be used as a solution to examine the experimental data on the path from the spherical to the rigid triaxial rotor.

The authors acknowledge financial support by the Scientific and Technical Research Council of Turkey (TUBITAK), under the project number TBAG (112T754).

References

1. F. Iachello, A. Arima, *The Interacting Boson Model* (Cambridge University Press, Cambridge, 1987).
2. J. Jolie, R.F. Casten, P. von Brentano, V. Werner, Phys. Rev. Lett. **87**, 162501 (2001).
3. J. Jolie, A. Linnemann, Phys. Rev. C **68**, 031301(R) (2003).
4. A. Bohr, Mat. Fys. Medd. Dan. Vid. Selsk. **26**, 14 (1952).
5. F. Iachello, Phys. Rev. Lett. **85**, 3580 (2000).
6. F. Iachello, Phys. Rev. Lett. **87**, 052502 (2001).
7. F. Iachello, Phys. Rev. Lett. **91**, 132502 (2003).
8. D. Bonatsos, D. Lenisa, D. Petrellis, P.A. Terziev, Phys. Lett. B **588**, 172 (2004).
9. J. Meng, W. Zhang, S.G. Zhou, H. Toki, L.S. Geng, Eur. Phys. J. A **25**, 23 (2005).
10. Z.Q. Sheng, J.Y. Guo, Mod. Phys. Lett. A **20**, 2711 (2005).
11. R. Fossion, D. Bonatsos, G.A. Lalazissis, Phys. Rev. C **73**, 044310 (2006).
12. D. Bonatsos, D. Lenis, D. Petrellis, P.A. Terziev, I. Yigitoglu, Phy. Lett. B **621**, 102 (2005).
13. D. Bonatsos, D. Lenis, D. Petrellis, P.A. Terziev, I. Yigitoglu, Phys. Lett. B **632**, 238 (2006).
14. I. Boztosun, D. Bonatsos, I. Inci, Phys. Rev. C **77**, 044302 (2008).
15. L. Fortunato, A. Vitturi, J. Phys. G Nucl. Part. Phys. **30**, 627 (2004).
16. L. Fortunato, S. De Baerdemacker, K. Heyde, Phys. Rev. C **74**, 014310 (2006).
17. D. Bonatsos, P.E. Georgoudis, N. Minkov, D. Petrellis, C. Quesne, Phys. Rev. C **88**, 034316 (2013).
18. I. Yigitoglu, D. Bonatsos, Phys. Rev. C **83**, 014303 (2011).
19. H. Sobhani, H. Hassanabadi, Nucl. Phys. A **957**, 177 (2017).
20. L. Naderi, H. Hassanabadi, Eur. Phys. J. Plus **131**, 5 (2016).
21. M. Chabab, A. El Batoul, A. Lahbas, M. Oulne, Nucl. Phys. A **953**, 158 (2016).
22. H.Sobhani, H. Hassanabadi, Mod. Phys. Lett. A **31**, 1650152 (2016).
23. P. Buganu, R. Budaca, Phys. Rev. C **91**, 014306 (2015).
24. P.M. Davidson, Proc. R. Soc. London, Ser. A **135**, 459 (1932).
25. A.F. Nikiforov, V.B. Uvarov, *Special Functions of Mathematical Physics* (Birkhaüser Basel, 1988).
26. D. Bonatsos, D. Lenis, N. Minkov, D. Petrellis, P.P. Raychev, P.A. Terziev, Phys. Lett. B **584**, 40 (2004).
27. D. Bonatsos, D. Lenis, N. Minkov, D. Petrellis, P.P. Raychev, P.A. Terziev, Phys. Rev. C **70**, 024305 (2004).
28. A.S. Davydov, A.A. Chaban, Nucl. Phys. **20**, 499 (1960).
29. J. Meyer-ter-Vehn, Nucl. Phys. A **249**, 111 (1975).
30. A.S. Davydov, G.F. Filippov, Nucl. Phys. **8**, 237 (1958).
31. A.S. Davydov, V.S. Rostovsky, Nucl. Phys. **12**, 58 (1959).
32. W. Greiner, *Quantum Mechanics: An Introduction* (Springer, Berlin, 1989).
33. L. Wilets, M. Jean, Phys. Rev. **102**, 788 (1956).
34. N.V. Zamfir, R.F. Casten, Phys. Lett. B **260**, 265 (1991).
35. E.A. McCutchan, D. Bonatsos, N.V. Zamfir, R.F. Casten, Phys. Rev. C **76**, 024306 (2007).
36. P. Cejnar, J. Jolie, R.F. Casten, Rev. Mod. Phys. **82**, 2155 (2010).